Korean J. Chem. Eng., 38(1), 152-162 (2021)
DOI: 10.1007/s11814-020-0661-8

pISSN: 0256-1115
eISSN: 1975-7220

Nickel-cobalt alloy coatings prepared by electrodeposition Part II: Morphology, structure, microhardness, and electrochemical studies

Rasha Muneer Al Radadi* and Magdy Ahmed Mahmoud Ibrahim,†**

*Chemistry Department, Faculty of Science, Taibah University, Al Madinah Al Mounwara, 30002 Saudi Arabia
**Chemistry Department, Faculty of Science, Ain Shams University, Abbassia, Cairo, 11566 Egypt
(*Received 3 May 2020 • Revised 8 August 2020 • Accepted 17 August 2020*)

Abstract−A study was carried out to synthesize Ni-Co alloy coatings electrochemically from complex acidic glycine (gly) bath. The impacts of some operating parameters such as Co^{2+} to Ni^{2+} concentration ratios in the bath, gly concentrations, pH, applied current, plating time and temperature on the morphology of Ni-Co alloy were investigated. The microstructure, microhardness, and electrochemical studies were also investigated. The electrochemical studies utilized cyclic voltammetry, anodic linear stripping voltammetry, and potentiostatic current-time transient techniques. It was realized that gly lowers the cathodic overvoltage for the Co^{2+} deposition while promoting cathodic overvoltage of Ni^{2+} deposition. Accordingly, the concurrent codeposition of Co^{2+} and Ni^{2+} ions was simplified. The morphology of Ni-Co alloy is significantly dependent on the operating parameters rather than on the bath composition. Moreover, increasing either pH or bath temperature produces Ni-Co deposits free from cracking. The roughness of the alloy is decreased in the presence of gly as shown by the atomic force microscope (AFM) study. In the presence of gly, the microhardness increases from 387 to 970 kg f mm^{-2}, i.e., it increased more than two-and-a-half times. On the other hand, X-ray diffraction analysis (XRD) data show that the crystallinity decreases with enhancing the percentage of cobalt in the deposits.

Keywords: Ni-Co Alloy, Anodic Stripping, Cyclic Voltammetry, Morphology, Microhardness, Potentiostatic Current Transients

INTRODUCTION

Ni-Co alloy possesses excellent adhesion and wear resistance, good hardness, corrosion resistance, and heat conductivity [1-4]. Moreover, these alloys are characterized by high magnetic properties [5,6]. Therefore, Ni-Co alloy coatings are used in various magnetic devices, especially in micro-technology for the manufacture of sensors, actuators, and memory devices [7,8]. The possible future applications of Ni-Co alloy coatings can be summarized as follows: Ni-Co multilayered magnetic nanowires can smooth the way for the next generation of data storage devices. Cantilever and probe tips for microscopy can be made of shaped electrodeposited Ni-Co. In the near future, Ni-Co film with modified surface morphologies is a good electrocatalyst for hydrogen evolution [9]. Therefore, Ni-Co alloy deposition has acquired the enormous interest of researchers. These alloys can be produced via different techniques such as electrowinning [10], ball milling, gas condensation, sol-gel [11], physical and chemical vapor deposition [12,13], sputtering and flame spraying [14-16] and electrodeposition. However, the electrodeposition technique has priorities over others. It is relatively inexpensive and carried out mostly at low (room) temperature [17]. The production rate is high with minimal size and shape limitations, and can be utilized to a different substrate [18].

The amount of cobalt in the alloy can be controlled by experimental parameters such as Ni^{2+}/Co^{2+} ratio in the bath, pH, temperature, agitation, deposition potential, or applied current as well as the addition agents. Consequently, the morphology, microstructure and, mechanical property of Ni-Co alloy can be modified. The impacts of various complexing agents such as, oxalic, malonic, succinic acids, citrate, gluconate, acetate, and glycine for nickel-cobalt electrodeposits have been investigated by several researchers [19-23]. Among them, gly has been used as a complexing agent for Ni, Co and Ni-Co alloy deposition [24-26], since gly has a good buffer characteristic and is able to keep the H^+ ions concentration constant at very adjacent to the cathode surface in the electrolytic process [27-34]. Moreover, electrolytic solutions containing gly have higher faradic efficiency and produce amorphous coatings [34]. Few investigations have properly handled nickel-cobalt codeposition in the presence of gly. Furthermore, the reported literature on the impact of gly on the morphology as well as on microhardness shows a lack of work. Therefore, the aim of the present paper was to continue our studies on the electrodeposition of Ni-Co alloy from gly bath and to evaluate the impact of Co^{2+} to Ni^{2+} concentration ratios in the bath, gly concentrations, pH, applied current and temperature on the morphology, microstructure, and microhardness.

EXPERIMENTAL DETAILS

Experiments were performed from electrolytic solutions containing $CoSO_4 \cdot 7H_2O$, $NiSO_4 \cdot 6H_2O$, H_3BO_3 and NH_2CH_2COOH (gly) (see Table 1). To study the effect of various $[Co^{2+}]/[Ni^{2+}]$ ratios in the bath on the electrodeposition process, various baths were estab-

†To whom correspondence should be addressed.
E-mail: magdyibrahim@sci.asu.edu.eg

Table 1. Composition of some Ni-Co alloy baths

Bath	Concentration (g/L)				pH	Ω (mS)
	$NiSO_4$	$CoSO_4$	H_3BO_3	Glycine		
Ni-Co 1	90	10	30	100	3.63	25.2
Ni-Co 2	80	20	30	100	3.68	24.8
Ni-Co 3	75	25	30	100	3.70	25.1
Ni-Co 4	70	30	30	100	3.71	25.1
Ni-Co 5	60	40	30	100	3.74	25
Ni-Co 6	50	50	30	100	3.78	24.8
Ni-Co 7	40	60	30	100	3.82	25
Ni-Co 8	30	70	30	100	3.86	25.1

lished using different ratios starting from 0.111 (Ni-Co 1 bath) to 2.33 (Ni-Co 8 bath) at constant concentrations of H_3BO_3 and gly as shown in Table 1. The electrolytic solutions used were prepared from analytical class chemicals and bi-distilled water. The topography of the Ni-Co alloy surfaces was checked with a Philips XL-40 FEG field emission SEM, while the structure of the Ni-Co deposits was identified by a Shimadzu XRD-6000 diffractometer (40 kV, 30 mA), Ni filter and CuKa radiation. A potentiostat/galvanostat SI 1287 Solartron, controlled by a personal computer, was utilized for the electrochemical measurements. The software packages, CorrWare 2 and CorrView2, provided by Solartron were used to trace and analyze the data. A schematic representation for the electrodeposition method is given in Fig. 1. A normal three-electrode cell was utilized for cyclic voltammetry (CV) tracing. The electrode acting as a working electrode was a glassy carbon electrode (GCE), a saturated calomel electrode (SCE) as a reference electrode and a Pt wire as a counter electrode. In the cathodic scan, the sweeping potential was initiated at a negative value and swept in a more negative direction. The scan was then reversed in the anodic direction up to the initial potential value. On the other hand, the anodic linear stripping voltammetry (ALSV) investigations were performed as published earlier [24,25]. The microhardness measurements were performed on some as-plated samples (the time of the plating was 60 min). In the microhardness measurements, a 25 gram-force was utilized and the indentations were established immediately on the coated sample. The microhardness of the electrodeposited coatings is commonly evaluated utilizing a traditional microhardness method employing a Vickers indenter (Hysitron TI 725 Ubi.). The medium of five readings recorded over the surroundings of a circle was considered as an estimation of the microhardness of the tested specimen. The data were expressed as Vicker's hardness number (VHN).

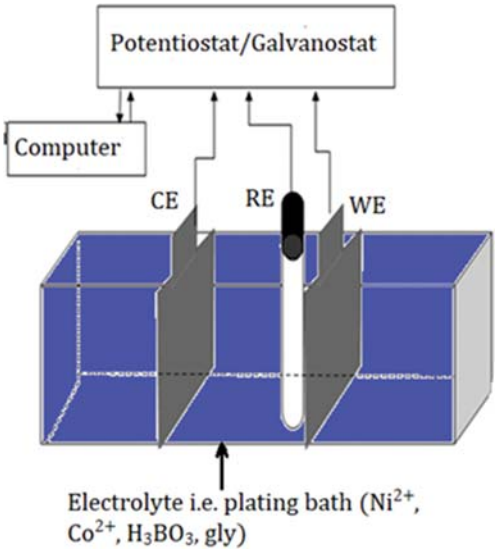

Fig. 1. A schematic diagram explaining electro-deposition method (WE: working electrode, CE: Counter electrode, RE: reference electrode).

RESULTS AND DISCUSSION

1. Cyclic Voltammetry

Fig. 2 shows the cyclic voltammograms (CVs) of single metal deposition of Ni, Co and Ni-Co alloy under comparable conditions. The data explores that the reduction peak of Ni-Co alloy lies in between those of Ni and Co. The increase in the slope of the cathodic part of the curves indicates the enhancement in the rate of deposition. This means that the rate of Ni deposition is higher than that of Co. On the other hand, the oxidation peak of Co was found to be higher than that of Ni or Ni-Co alloy, indicating that the Co

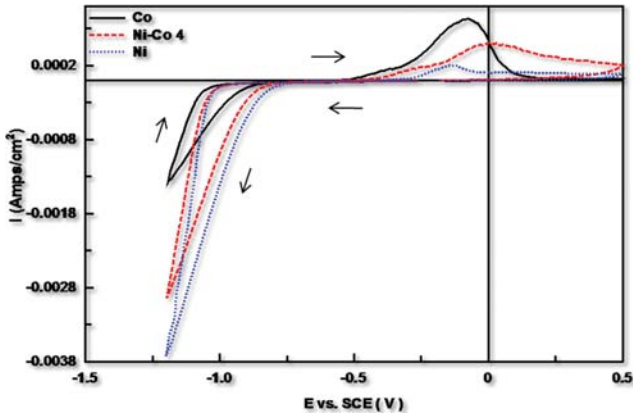

Fig. 2. Cyclic voltammetric curves recorded at GCE for deposition of Co, Ni and Ni-Co alloy from baths containing: 100 g/L gly, 30 g/L H_3BO_3, scan rate 100 mV s^{-1}.

will be preferentially deposited under such circumstances. The CV of Ni displays two peaks, a sharp cathodic peak at −1.2 V_{SCE} represents the reduction of Ni^{2+} to Ni^0 and an anodic peak at −0.15 V_{SCE} represents the Ni dissolution. On the other hand, the CV of Co exhibits a sharp cathodic peak at −1.25 V_{SCE} analogous to the reduction of Co^{2+} to Co^0 and an oxidation peak at −0.08 V_{SCE} represents the Co dissolution. On the other hand, the voltammogram of the alloy explores one reduction peak at −1.22 V corresponding to the codeposition of Co^{2+} and Ni^{2+} ions and a broad anodic peak at 0.0 V_{SCE} equivalent to the concurrent dissolution of cobalt and nickel. Note that the anodic oxidation peak of Ni is smaller than that of Co or Ni-Co alloy, indicating that the Ni will be present in a small amount in the alloy.

Fig. 3 shows typical CVs of the Ni-Co alloy from solutions containing various $[Co^{2+}]/[Ni^{2+}]$ ratios. The data shows that the reduction peak is not affected by changing the $[Co^{2+}]/[Ni^{2+}]$ ratios in the electrolytic bath. However, the anodic oxidation peak heights increased with increasing this ratio due to the increase in the Co percent in the deposit. The oxidation peak moves to the less noble potentials as the percentage of cobalt in the solution enhances. The obvious broadening of the oxidation peak for Ni-Co 2 and Ni-Co 4 baths indicates the slow rate of Ni and Co dissolution from the deposited alloy. Furthermore, the presence of cross-over of the cathodic and anodic scans is noticeable, indicating a new phase formation involving nucleation followed by diffusion-limitation [33].

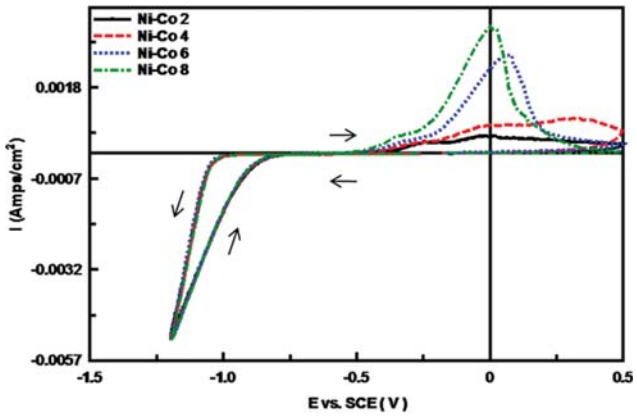

Fig. 3. Cyclic voltammetric curves recorded at GCE for various $[Co^{2+}]/[Ni^{2+}]$ ratios in the baths (100 g/L gly, 30 g/L H_3BO_3), scan rate 100 mV s^{-1}.

Fig. 4 depicts the influence of gly concentration on the CVs of Ni-Co alloy. The observed cathodic peaks were moved slightly towards the more negative potentials as a result of complexation and could be due to the adsorption of gly [27]. It was realized that gly lowered the cathodic overvoltage for the Co^{2+} deposition while promoting the cathodic overvoltage of Ni^{2+} deposition. Accordingly, the concurrent codeposition of Co^{2+} and Ni^{2+} ions was simplified. On the other hand, the anodic oxidation peak heights were decreased with increasing gly concentration and the peak became very broad. Our previous work [24] concluded that the complex formed between Ni^{2+} and gly activates the electroreduction of Ni^{2+} ions. This implies also that glycine acts as an accelerator for nickel reduction over the copper surface and does not block the active sites on the electrode surface for nickel deposition. In contrast, the deposition of Co^{2+} is markedly inhibited by complex formation. The liberation of Co^{2+} from glycine at the cathode is slow due to a strong interaction between Co^{2+} and glycine [25].

Fig. 5 explores the impact of pH (pH 3.0-8.1) of the electrolytic solution containing cobalt, nickel, and gly on the cyclic vo1tammetric responses. Investigation of the results in Fig. 4 explains that increasing pH moved the reduction peak in the cathodic scan to the more negative potential value well consistent with the data of the polarization behavior illustrated previously in [26]. This is more noticeable when the pH is higher because, at higher pH, the level of complexation is also high. In the case of low pH, the reduction potential shift is affected by H^+ ions, while it is influenced by OH^- ions in the case of higher pH values. Fig. 5 explores that in-

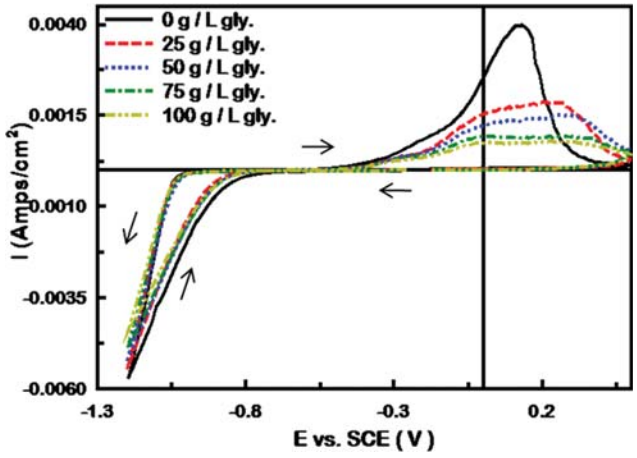

Fig. 4. Cyclic voltammograms recorded at GCE during Ni-Co alloy deposition from bath containing: 70 g/L $NiSO_4$, 30 g/L $CoSO_4$, 30 g/L H_3BO_3 at different gly concentrations, scan rate 100 mV s^{-1}.

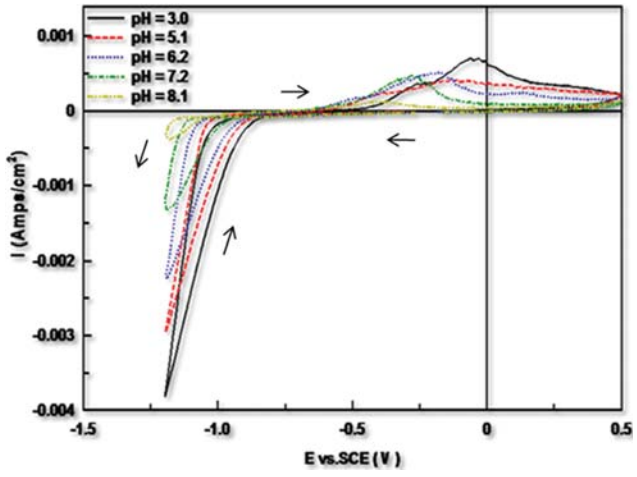

Fig. 5. Cyclic voltammograms recorded at GCE during Ni-Co alloy electrodeposition from bath containing: 70 g/L $NiSO_4$, 30 g/L $CoSO_4$, 30 g/L H_3BO_3 and 100 g/L gly at different pH values, scan rate 100 mV s^{-1}.

creasing pH leads to a decline in the anodic peak. It could be realized that an increase in pH leads to a decline in the rate of alloy deposition, leading to a noticeable decline in the area of dissolution peaks. The peak height is expressive of the amount of the given phase in the deposited coat. Hence, with increasing the pH value, the amount of Ni-Co declines as specified by the relative decline in the heights of the anodic peaks in the CVs.

2. In Situ-anodic Linear Stripping Voltammetry (ALSV)

Under anodic overvoltage conditions, the distinct components of an alloy tend to dissolve at different potentials, and the distribution of voltammetric peaks is characteristic for each alloy structure. The peak currents depend on the film thickness, while their number and potential depend only on the alloy structure. A typical ALSV for Ni-Co alloy codeposited on the GCE at various plating conditions is shown in Figs. 6-8. The alloy was deposited at $-1.22\ V_{SCE}$ for 100 s. For comparison, stripping voltammograms for pure Ni, pure Co and Ni-Co alloy were performed at similar experimental circumstances (Fig. 6). Each voltammogram contains a single dissolution peak. The appearance of a dissolution peak for the Ni-Co deposit indicates that the Co and Ni components of the deposit dissolved concurrently. Nonetheless, the stripping charge (the area under the peak) might be taken as a quantitative estimation of the current efficiency of metal deposition. It is noticeable that the stripping charge of pure Ni is very low as compared to that of pure Co and the Ni-Co deposit. These outcomes affirm the assumption that cobalt-rich deposit is produced from these electrolytic solutions at room temperature.

A group of ALSV responses for the alloy deposited from various $[Co^{2+}]/[Ni^{2+}]$ ratios in the electrolytic solution was performed and the data are given in Fig. 7. The results show that the amount of electricity used at the anodic peak potential increases with iincreasing Co^{2+} concentration or increasing $[Co^{2+}]/[Ni^{2+}]$ ratio in the bath. The stripping peak potential is considerably moved to the less noble potential with enhancing $[Co^{2+}]/[Ni^{2+}]$ ratios in the electrolytic solution. According to Fig. 7, the alloy containing higher Co content is more easily oxidized than that containing less Co content.

Fig. 8 describes the influence of the inclusion of various gly concentrations (0-100 g/L) into the electrolytic solution on the stripping voltammograms. The inclusion of gly into the electrolytic solution decreased the stripping charge of the Ni-Co deposition and then decreased the current efficiency of the alloy deposition, inconsistent with our previous work [26]. This indicates that the plating process is inhibited in the presence of gly. The appearance of two anodic oxidation peaks in the anodic response, especially in the presence of gly, could probably be due to the dissolution of the alloy from different phases, which cannot be detected using XRD since the alloy is not well crystalline. The ALSV responses during Ni-Co alloy codeposition at various pH were carried out and it was found that increasing the pH enhances both the stripping current and the area under the peak (data are not shown here).

3. Potentiostatic Current-time Transients

Potentiostatic i-t transients have some usefulness over CV when utilized to study the kinetics of nucleation and its growth. The nucleation takes place at a definite deposition potential, defining constant values of the nucleation work and the rate of charge transfer for the whole surface of an energy-regular electrode during interval time. For this objective, a group of i-t transients at a specified deposition potential, for Ni-Co alloy deposition onto GCE

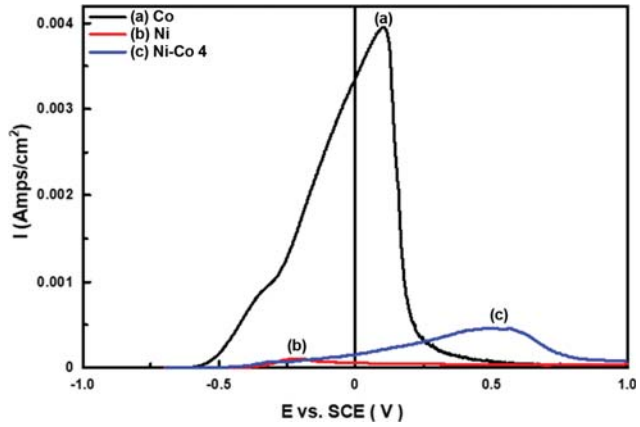

Fig. 6. In-situ anodic linear stripping voltammetric curves for Co, Ni and Ni-Co alloy (E=−1.22 V, t=100 s, scan rate 10 mV s^{-1}).

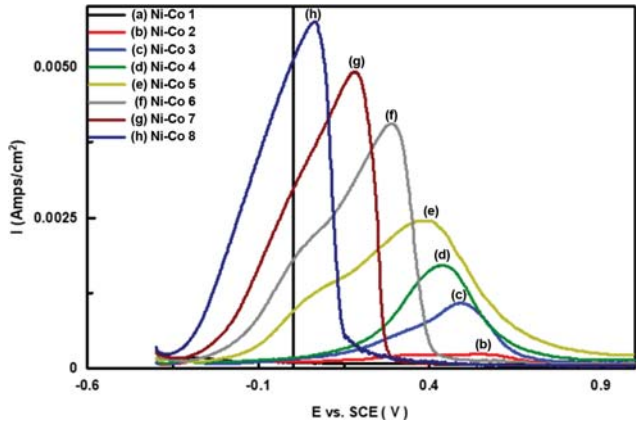

Fig. 7. In-situ anodic linear stripping voltammetric curves for Ni-Co alloy deposited from baths with various $[Co^{2+}]/[Ni^{2+}]$ ratios (E=−1.22 V, t=100 s, scan rate 10 mV s^{-1}).

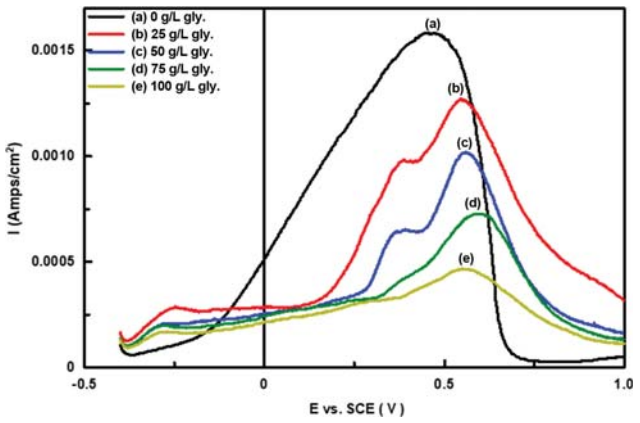

Fig. 8. In-situ anodic linear stripping voltammetric curves of Ni-Co alloy deposition with various concentrations of gly (E=−1.22 V, t=100 s, scan rate 10 mV s^{-1}).

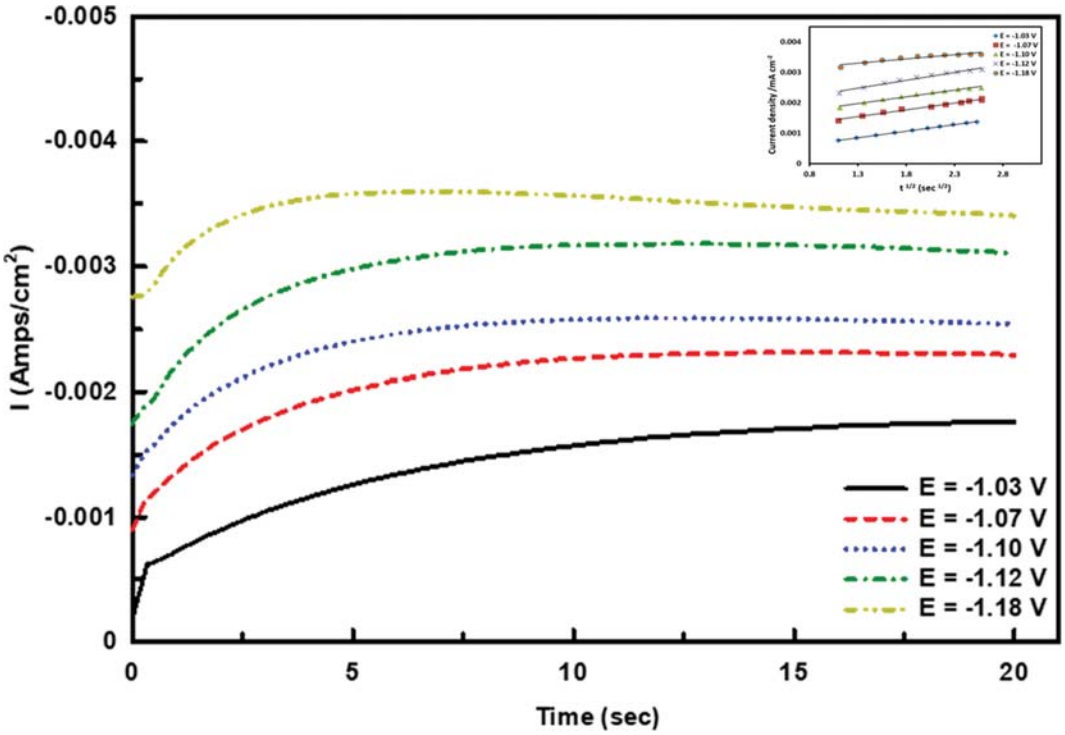

Fig. 9. Potentiostatic current-time transients during Ni-Co alloy electrodeposition from bath containing: 100 g/L $NiSO_4$, 100 g/L $CoSO_4$, 30 g/L H_3BO_3 and 100 g/L gly at different values of deposition potentials, t=20 s, insert is the relationship between current density and $t^{1/2}$ during Ni-Co alloy electrodeposition at various deposition potentials.

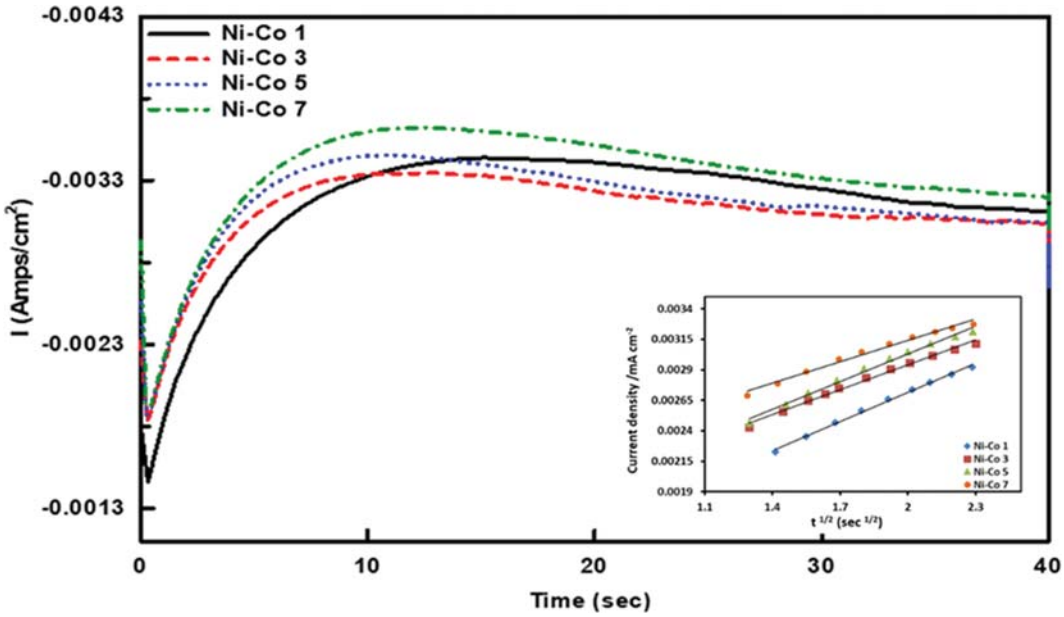

Fig. 10. Potentiostatic current-time transients for different $[Co^{2+}]/[Ni^{2+}]$ ratios in the baths during Ni-Co alloy electrodeposition from bath containing: 30 g/L H_3BO_3, 100 g/L gly, E=−1.1 V, t=100 s, insert is the relationship between current density and $t^{1/2}$ during Ni-Co alloy electrodeposition at various $[Co^{2+}]/[Ni^{2+}]$ ratios in the bath.

under different operating conditions, were measured and results are presented in Figs. 9, 10.

Fig. 9 presents typical potentiostatic i-t transients for Ni-Co alloy deposition at various deposition potentials. It is seen that the current increases quickly to a limiting or steady-state value. Transients are distinguished for the nucleation and phase growth of metal on glassy carbon. Moreover, the data suggest that nucleation growth is not a diffusion-controlled process. The ascending part of the curve

explores the enhancement in current as the electroactive area is enhanced either as instantaneous growth (each independent nucleus grows in size) and/or as progressive growth (the number of nuclei increases). The current transients flatten off when the surface becomes filled [32]. The small variation of the steady-state current with time suggests that after overlapping of the growth nuclei and formation of a ceaseless coating thickening occurs under limited diffusion control. The steady-state current is enhanced as the deposition potential is made more negative. Hydrogen evolution again occurs, but the current for this side reaction serves only to magnify the response without changing its shape.

The rising portions of the transients were analyzed by drawing i against $t^{1/2}$, whereby straight lines were obtained as shown in Fig. 9 inset. This indicates that the Ni-Co alloy is created by a mechanism where instantaneous nucleation is followed by 3D growth under charge transfer control [35,36]. This means that the formation of fresh nuclei is arrested at a very early stage. The slopes of these plots are proportional to the rate constant for charge transfer.

Fig. 10 shows the potentiostatic i-t transients at a constant deposition potential of $-1.1\ V_{SCE}$ for Ni-Co deposition from different $[Co^{2+}]/[Ni^{2+}]$ ratios in the bath. Analysis of the rising portion of the i-t curves (Fig. 10 inset) produces straight lines which indicate also that whatever this ratio in the bath, the Ni-Co deposit is formed by a mechanism where instantaneous nucleation is followed by 3D growth under charge transfer control.

4. Characterization of Ni-Co Alloy Deposits

4-1. Surface Morphology

The addition of gly to the electroplating bath of Ni-Co deposition produces bright deposits characterized by high adhesion to the copper substrate. The surface morphology of the as-plated coating of Ni-Co deposited from gly-free solutions shows circular grains of different sizes which covered the entire cathode surface (Fig. 11). It is observed that the deposit obtained from a gly-free solution is free from cracking. However, most of the deposits prepared from solutions containing gly exhibit extensive microcracking on the surface. This could be due to the observed tensile stress result from the H_2 evolution. The tensile stress could be easily detected by plating from these baths for a long time. The addition of a low concentration of gly (25 g/L) into the electrolytic solution increased the formation rate of crystallite nucleation on the substrate. Further increase in gly concentration in the bath (25-150 g/L) produced intense microcracks (Fig. 11).

Generally, from the data shown in Figs. 11 and 12 the morphology of Ni-Co alloy is strongly dependent on the operating conditions rather than on the bath compositions. For example, all the deposits obtained from Ni-Co 1 bath to Ni-Co 8 bath have the same morphology (Fig. 12). These results indicate that the change in the $[Co^{2+}]/[Ni^{2+}]$ ratio in the bath or the gly concentrations has no significant effect on the morphology. However, changing the operating conditions, e.g., current density, temperature and pH produced deposits that possess different morphology. For example, increasing the current density from 6.7 to 33.3 mA cm^{-2} (Fig. 13) leads to the formation of a cauliflower-like structure which increased in size with an increase in current density. However, raising pH from pH 3.0 to pH 8.1 (Fig. 14) decreased the cracking of the deposit and this could be due to the decrease in the rate of H_2

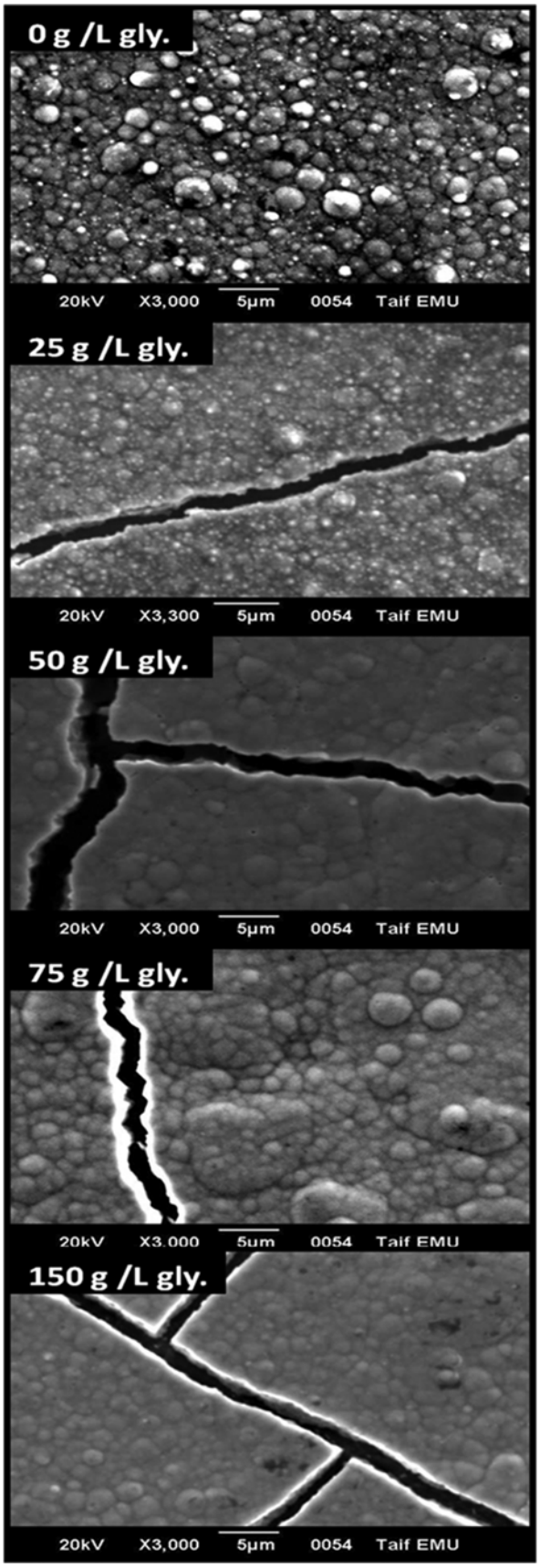

Fig. 11. SEM photomicrographs of Ni-Co 4 deposited at various gly concentrations.

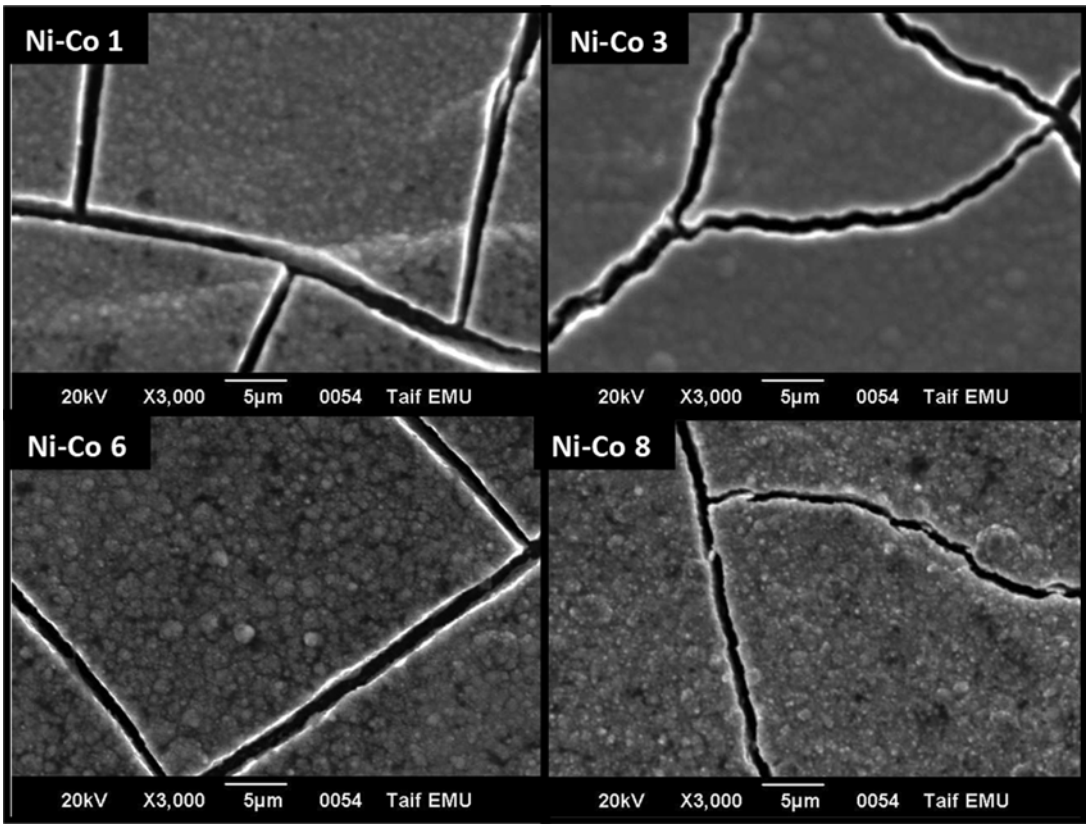

Fig. 12. SEM photomicrographs of Ni-Co alloy deposited at various $[Co^{2+}]/[Ni^{2+}]$ ratios in the bath.

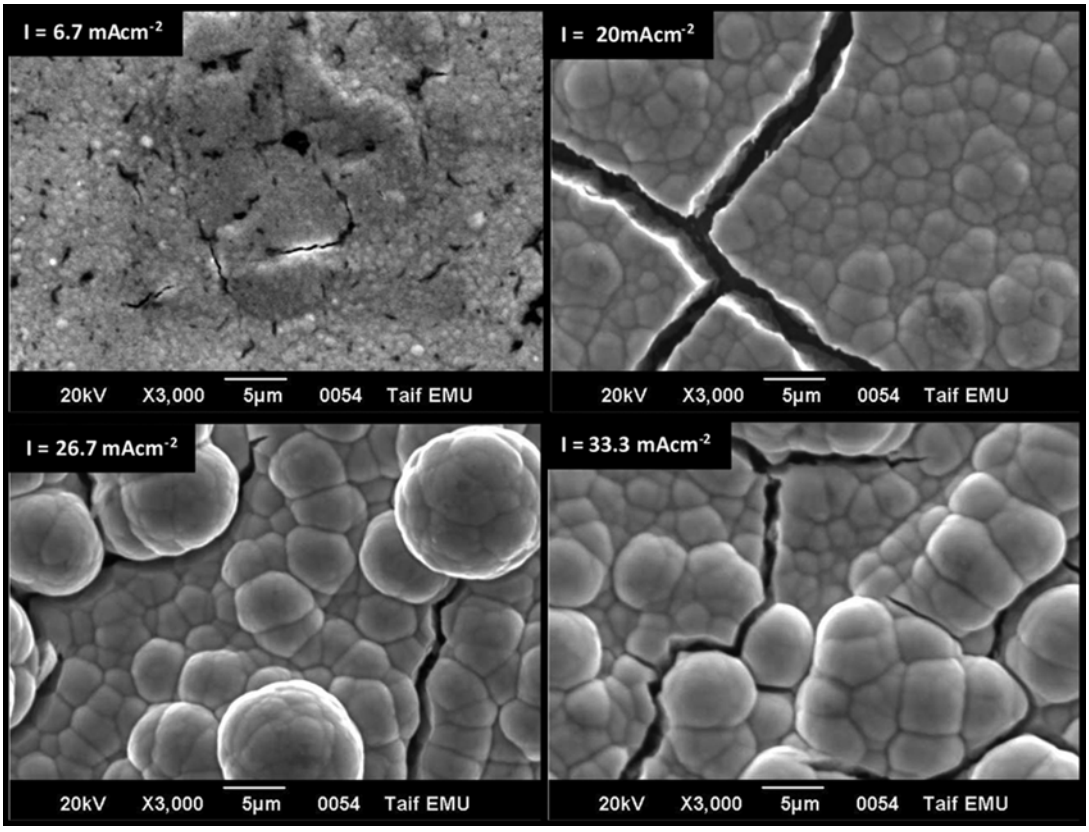

Fig. 13. SEM photomicrographs of Ni-Co 4 deposited at various current density.

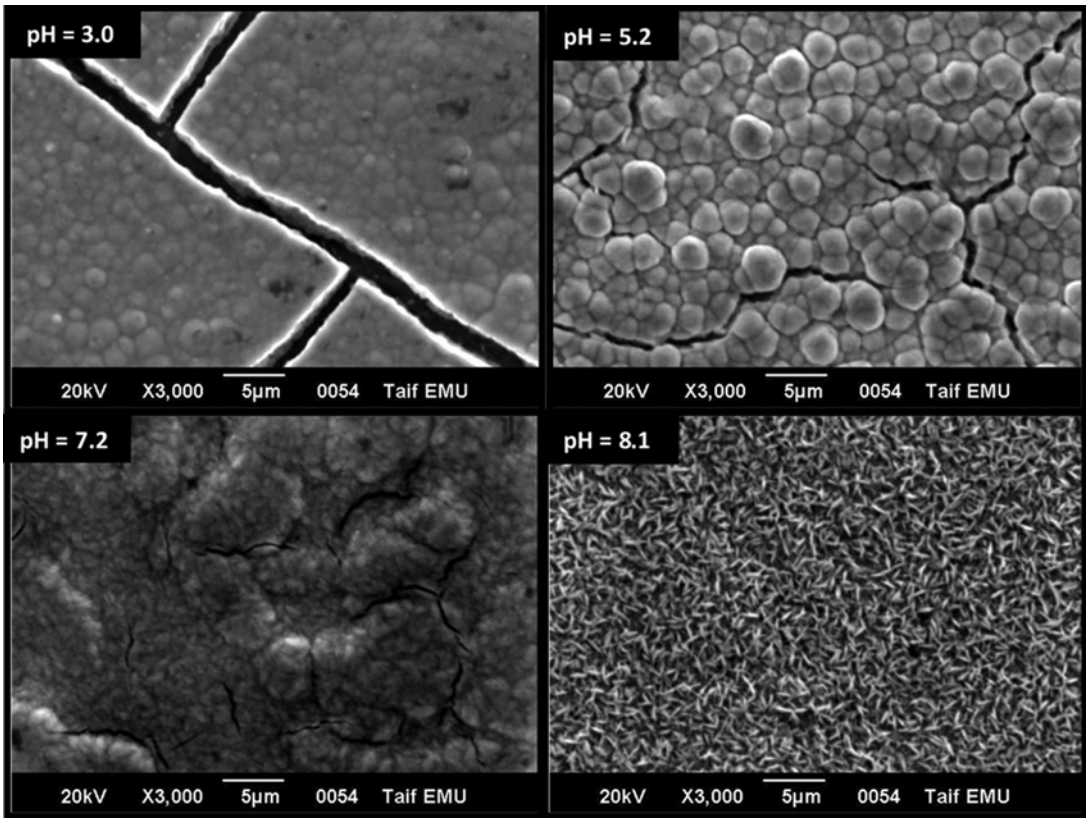

Fig. 14. SEM photomicrographs of Ni-Co 4 deposited at various pH.

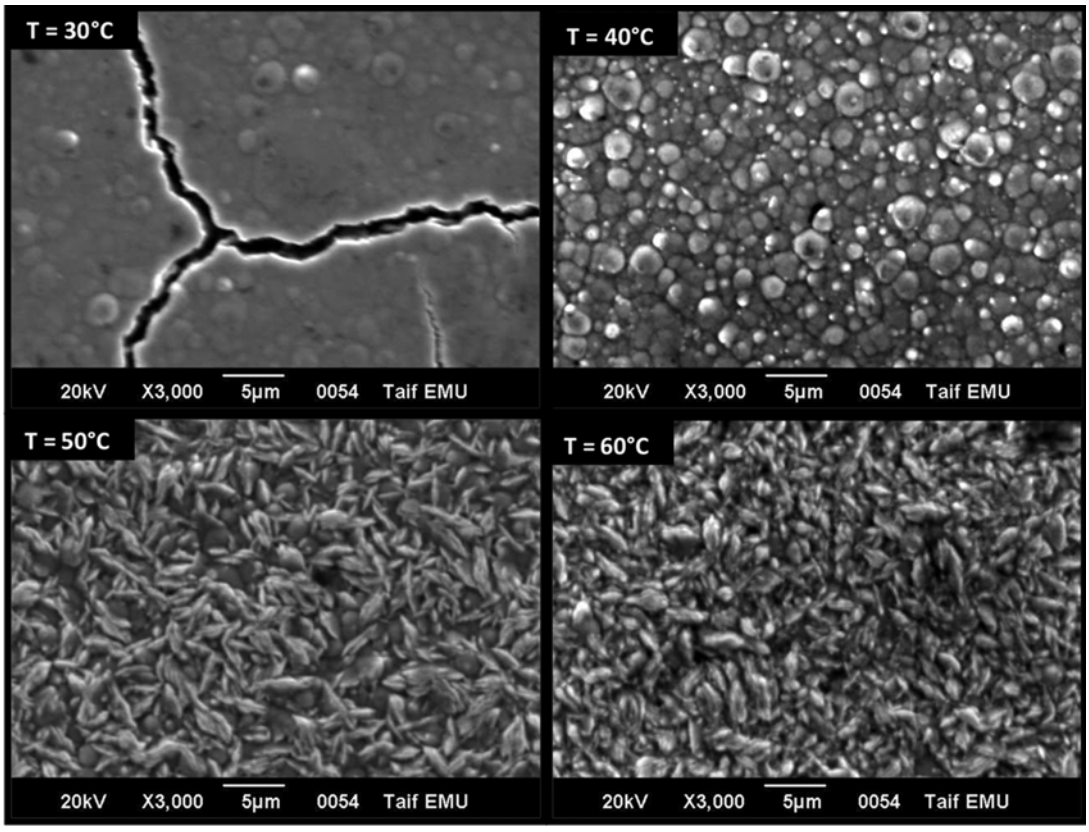

Fig. 15. SEM photomicrographs of Ni-Co 4 deposited at various bath temperature.

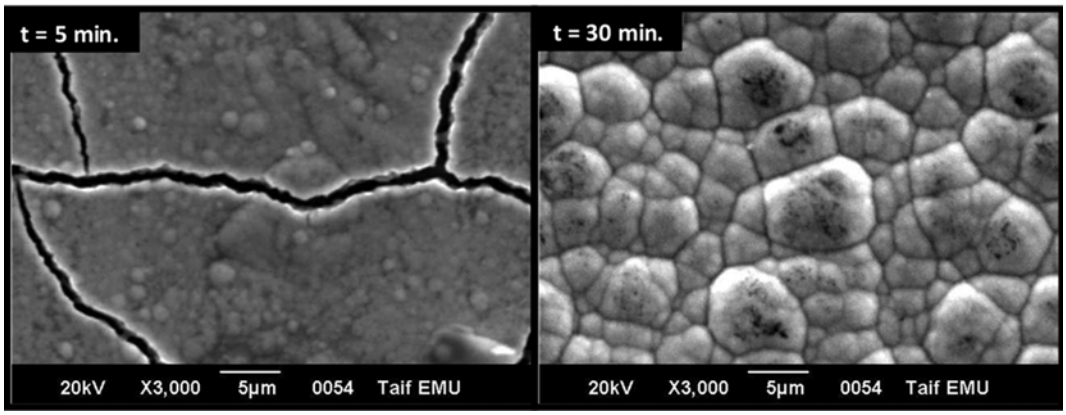

Fig. 16. SEM photomicrographs of Ni-Co 4 deposited at various deposition time.

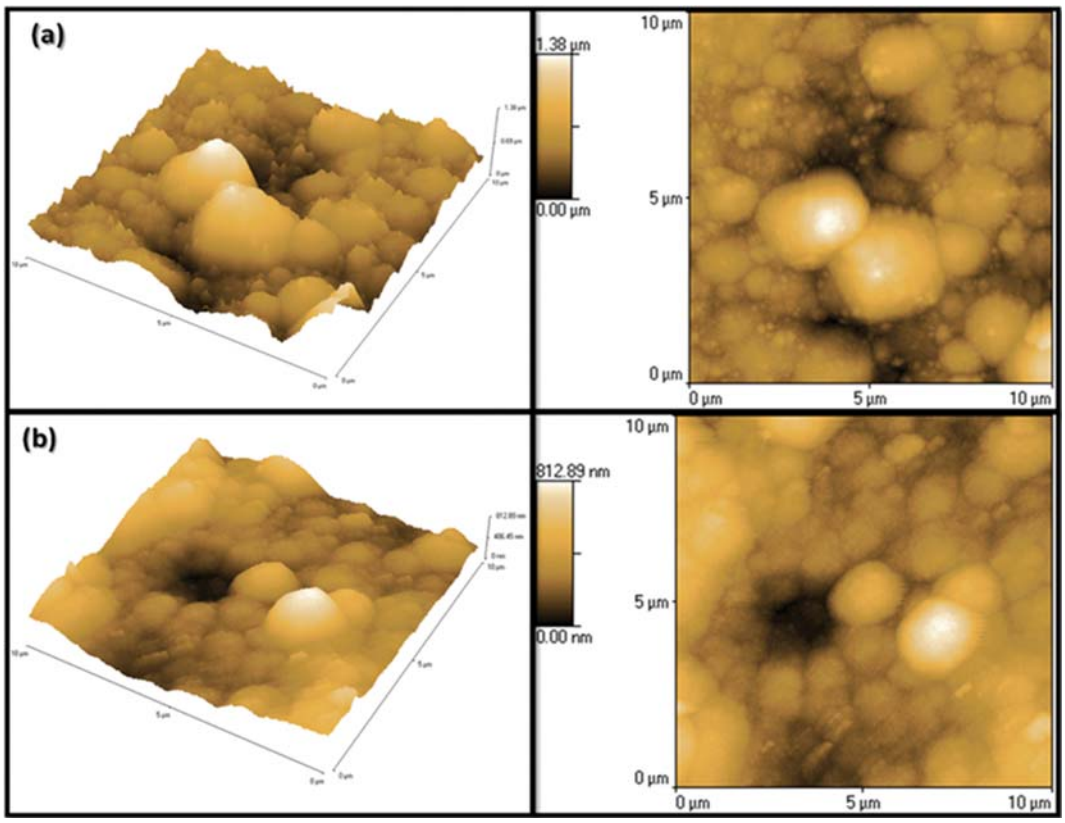

Fig. 17. AFM images of the Ni-Co alloy deposited in the absence and presence of gly concentrations (a) 0 g/L gly, (b) 75 g/L gly.

evolution. This is clear from the photomicrograph at pH 8.0 that exhibits a drastic change in morphology where very fine grains in elongated shape (in nanosized) free from cracking were obtained.

On the other hand, increasing bath temperatures shows that the cracking is completely disappeared starting from bath temperature of 40 °C, and a drastic change in morphology is observed with the further increase of temperature (Fig. 15). The alloy grains changed from circular grains to very fine grains. Note that increasing either pH or bath temperature produced Ni-Co deposits free from cracking.

The effect of plating time (5.0-30 min) on the surface morphology of Ni-Co deposits was investigated and the data are shown in Fig. 16. Increasing the duration of plating increased the agglomeration of the alloy grains. It is also noticeable that at 30 min the cracks completely disappeared. As a conclusion, increasing the plating time or current density resulted in the establishment of clusters of agglomerated grains. Therefore, enhancing either pH or bath temperature produced very fine grains.

On the other hand, Fig. 17 shows the AFM images of the Ni-Co electrodeposited from bath free from gly and bath containing gly. It is found that the alloy is deposited as three-dimensional nuclei that are randomly distributed over the copper substrate surface in different sizes. Moreover, the roughness of the alloy deposit decreases

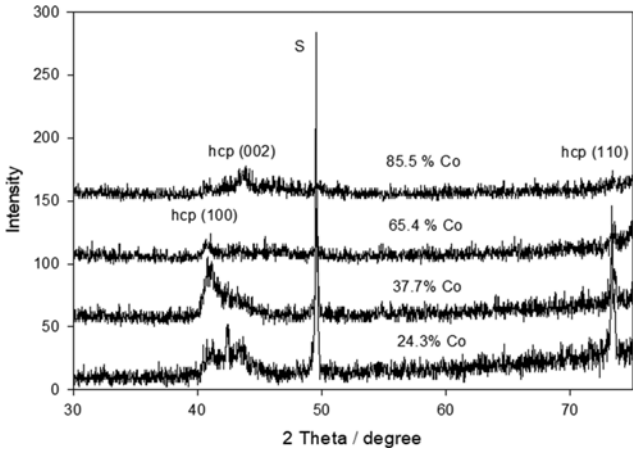

Fig. 18. X-ray diffraction analysis of Ni-Co alloy deposited with various Co content in the alloy.

in the presence of gly from 1.38 μm to 812.9 nm. Simultaneously, the coatings tend to be more compact and have smaller size nuclei.

4-2. XRD Analysis

X-ray analysis does not always permit identifying the phases present in the coating [37]. Several Ni-Co electrodeposition investigations [9] have concluded that various properties, microstructure, and phase structure, of these alloys are a function of the Co content of the coating, which is controlled by deposition parameters such as pH, temperature, electrolyte composition, and the applied current. The XRD data shows that the Ni-Co alloy deposited from gly-containing solution is characterized by a low degree of crystallinity as presented in Fig. 18. The outcomes specify that the Ni-Co alloy prepared from gly-containing solution exhibited three peaks corresponding to the following hexagonal close-packed (hcp) phases: (100) at 2θ=40.9° and (002) at 2θ=43.8° and (110) at 2θ=73.3°, respectively. Generally, the degree of crystallinity decreases with an increasing percentage of cobalt in the deposits. This is clear from the diffractograms at higher Co content of 65.4 and 85.5%. In fact, most of the Ni-Co alloy deposited from other baths are well crystalline and exhibit sharp peaks in the XRD diffractograms [19,38,39].

4-3. Microhardness of Ni-Co Alloy

The Vickers microhardness Hv (kg f mm^{-2}) for some as-plated Ni-Co alloy electrochemically formed from gly-containing and gly-free solutions was determined. The results indicate that the microhardness of the alloy formed from gly solutions is greater than the microhardness of the alloy formed from gly-free solutions. It was observed that the hardness of Ni-Co alloy from gly free solution was 387 kg f mm^{-2}. The inclusion of 50 g/L gly enhances greatly the microhardness to be 970 kg f mm^{-2} (Table 2), i.e., the microhardness is increased more than two-and-a-half times in the presence of gly. Further inclusion of 100 g/L gly shows that the hardness is still high (962 kg f mm^{-2}). These values are much higher than that reported for some other cobalt alloys deposited under similar conditions [22,24,40]. For example, Hagarova et al. reported a value of 556 Hv as a maximum value of Ni-Co alloy deposited from sulfate-chloride bath [41]. On the other hand, Ma et al. showed that the microhardness of nanocrystalline Ni-Co coating formed from chloride solutions was in the range of 300-500 HV relying on the Co percentage [42].

Table 2. Microhardness of Ni-Co coatings in the absence and presence of gly

[gly]/g/L	Hv/kg f mm^{-2}
0	387
50	970
100	962

CONCLUSIONS

The morphology, structure, and microhardness of Ni-Co deposits prepared from gly electrolytes were studied as a function of gly ion concentration, which acts as a complexing agent during the electrodeposition process. It was realized that gly lowers the cathodic overvoltage for the Co^{2+} deposition and promotes cathodic overvoltage of Ni^{2+} deposition. Accordingly, the concurrent codeposition of Co^{2+} and Ni^{2+} ions was simplified. The morphology of Ni-Co alloy is strongly dependent on the operating conditions rather than on the bath compositions. Increasing either pH or bath temperature produced very fine grains of Ni-Co deposits free from cracking. The potentiostatic current-time curves show that the Ni-Co alloy deposit is formed by a mechanism where instantaneous nucleation is followed by 3D growth under charge transfer. On the other hand, XRD data show that the crystallinity decreases with enhancing the percentage of cobalt in the deposits. Moreover, in the presence of gly, the microhardness increases greatly from 387 to 970 kg f mm^{-2}, i.e., more than two-and-a-half times. Additional research is required to better understand the microstructure and properties of Ni-Co coatings and to develop further coatings with improved characteristics such as wear and corrosion resistance. In the present study, the microhardness was high enough, and the Ni-Co coating is a candidate to replace hard chromium coating.

REFERENCES

1. G. F. Wang, K. C. Chan and K. F. Zhang, *Scr. Mater.*, **54**, 765 (2006).
2. L. M. Chang, M. Z. An, H. F. Guo and S. Y. Shi, *Appl. Surf. Sci.*, **253**, 2132 (2006).
3. L. P. Wang, Y. Gao and Q. J. Xue, *Appl. Surf. Sci.*, **242**, 326 (2005).
4. G. Y. Qiao, T. F. Jing and N. Wang, *Electrochim. Acta*, **51**, 85 (2005).
5. S. Vasefi and M. Parrari, *Korean J. Chem. Eng.*, **27**(2), 422 (2010).
6. H. Park, K. M. Kim, H. Kim, D.-K. Kim, Y. S. Won and S.-K. Kim, *Korean J. Chem. Eng.*, **35**(7), 1547 (2018).
7. D. Golodnitsky, Y. Rosenberg and A. Ulus, *Electrochim. Acta*, **47**, 2707 (2002).
8. D. Kim, D. Y. Park, B. Y. Yoo, P. T. A. Sumodjo and N. V. Myung, *Electrochim. Acta*, **48**, 819 (2003).
9. A. Karimzadeha, M. Aliofkhazraeia and F. C. Walsh, *Surf. Coat. Technol.*, **372**, 463 (2019).
10. C. Lupi and D. Dilone, *Miner. Eng.*, **14**(11), 1403 (2001).
11. J. Idris, C. Christian and E. Gaius, *J. Nanomaterials*, **2013**, 1 (2013).
12. A. N. Correia and S. A. S. Machado, *J. Appl. Electrochem.*, **33**, 367 (2003).

13. M. Schwartz, N. V. Myung and K. Nobe, *J. Electrochem. Soc.*, **151**(7), C468 (2004).
14. L. Tian, J. Xu and C. Qiang, *Appl. Surf. Sci.*, **257**, 4689 (2011).
15. M. Farzaneh, M. Zamanzad-Ghavidel, K. Raeissi, M. Golozar, A. Saatchi and S. Kabi, *Appl. Surf. Sci.*, **257**, 5919 (2011).
16. H. El-Feky, M. Negem, S. Roy, N. Helal and A. Baraka, *Sci. China. Chem.*, **56**(10), 1446 (2013).
17. A. Sanaty-Zadeh, K. Raeissi and A. Saidi, *J. Alloys Compd.*, **485**(1-2), 402 (2009).
18. G. Qiao, T. Jing, N. Wang, Y. Gao, X. Zhao, J. Zhou and W. Wang, *J. Electrochem. Soc.*, **153**(5), C305 (2006).
19. E. Gomez, S. Pane and E. Valles, *Electrochim. Acta*, **51**, 146 (2005).
20. E. Gomez, E. Pellicer and E. Valles, *J. Electroanal. Chem.*, **580**, 222 (2005).
21. D. Golodnitsky, N. V. Gudin and G. A. Volyanuk, *J. Electrochem. Soc.*, **147**(11), 4156 (2000).
22. S. Hassani, K. Raeissi and M. A. Golozar, *J. Appl. Electrochem.*, **38**, 689 (2008).
23. J. Vijayakumar, S. Mohan and S. S. Yadav, *J. Alloys Compd.*, **509**, 9692 (2011).
24. M. A. M. Ibrahim and R. M. Al Radadi, *Int. J. Electrochem. Sci.*, **10**, 4946 (2015).
25. M. A. M. Ibrahim and R. M. Al Radadi, *Mat. Chem. Phys.*, **151**, 222 (2015).
26. R. M. Al Radadi and M. A. M. Ibrahim, *Korean J. Chem. Eng.*, in press.
27. O. A. Taranina, N. V. Evreinova, I. A. Shoshina, V. N. Naraev and K. I. Tikhonov, *Russ. J. Appl. Chem.*, **83**(1), 58 (2010).
28. Y. Zhang, L. Feng and W. Qiu, *J. Mater. Sci.*, **54**, 9507 (2019).
29. M. H. Gharahcheshmeh and M. H. Sohi, *J. Appl. Electrochem.*, **40**, 1563 (2010).
30. J. C. Wei, M. Schwartz and K. Nobe, *J. Electrochem. Soc.*, **155**, D660 (2008).
31. T. Boiadjieva, D. Kovacheva, L. Lyutov and M. Monev, *J. Appl. Electrochem.*, **38**, 1435 (2008).
32. U. Lačnjevac, B. M. Jović and V. D. Jović, *J. Electrochem. Soc.*, **159**(5), D310 (2012).
33. Y. Messaoudi, N. Fenineche, A. Guittoum, A. Azizi, G. Schmerber and A. Dinia, *J. Mater. Sci. Mater. Electron.*, **24**, 2962 (2013).
34. E. A. Abd El Maguid, S. S. Abd El Rehim and E. M. Mostafa, *Trans. IMF*, **77**, 188 (1999).
35. C. Q. Cui, S. P. Jiang and A. C. C. Tseung, *J. Electrochem. Soc.*, **137**, 3418 (1990).
36. S. Swathirajan, *J. Electrochem. Soc.*, **133**, 671 (1986).
37. R. Fratesi, G. Roventi, G. Giuliani and C. R. Tomachuk, *J. Appl. Electrochem.*, **27**, 1088 (1997).
38. C. Lupi, A. Dellera, M. Pasquali and P. Imperatori, *Surf. Coat. Technol.*, **205**, 5394 (2011).
39. I. Kharmachi, L. Dhouibi, P. Berçot and M. Rezrazi, *J. Mater. Environ. Sci.*, **7**(5), 1670 (2016).
40. S. S. Abd El Rehim, M. A. M. Ibrahim, M. M. Dankeria and M. Emad, *Trans. IMF*, **80**(3), 105 (2002).
41. M. Hagarova, D. Jakubeczyova and J. Cervova, *Int. J. Electrochem. Sci.*, **10**, 9968 (2015).
42. C. Ma, S. C. Wang and F. C. Walsh, *Trans IMF*, **93**(2), 104 (2015).